

PAPER

## Measurement of the passive fast-ion D-alpha emission on the NSTX-U tokamak




To cite this article: G Z Hao *et al* 2018 *Plasma Phys. Control. Fusion* **60** 025026

View the [article online](#) for updates and enhancements.

### Related content

- [Measurement and simulation of passive fast-ion D-alpha emission from the DIII-D tokamak](#)  
Nathan G. Bolte, William W. Heidbrink, David Pace *et al.*
- [Analysis of fast-ion D data from the National Spherical Torus Experiment](#)  
W.W. Heidbrink, E. Ruskov, D. Liu *et al.*
- [Fast-ion transport in low density L-mode plasmas at TCV using FIDA spectroscopy and the TRANSP code](#)  
B Geiger, A N Karpushov, B P Duval *et al.*

# Measurement of the passive fast-ion D-alpha emission on the NSTX-U tokamak

G Z Hao<sup>1</sup> , W W Heidbrink<sup>1</sup>, D Liu<sup>1</sup> , M Podesta<sup>2</sup> , L Stagner<sup>1</sup>, R E Bell<sup>2</sup>, A Bortolon<sup>2</sup>  and F Scotti<sup>3</sup>

<sup>1</sup>University of California, Irvine, CA 92697, United States of America

<sup>2</sup>Princeton Plasma Physics Laboratory, Princeton, NJ 08540, United States of America

<sup>3</sup>Lawrence Livermore National Laboratory, Livermore, CA 94550, United States of America

E-mail: [ghao@pppl.gov](mailto:ghao@pppl.gov)

Received 9 September 2017, revised 30 November 2017

Accepted for publication 7 December 2017

Published 8 January 2018



CrossMark

## Abstract

On National Spherical Torus Experiment Upgrade, the passive fast-ion D-alpha (passive-FIDA) spectra from charge exchange (CX) between the beam ions and the background neutrals are measured and simulated. The results indicate that the passive-FIDA signal is measurable and comparable to the active-FIDA on several channels, such as at the major radius  $R = 117$  cm. Here, active-FIDA means the active D-alpha emission from the fast ions that CX with the injected neutrals. The shapes of measured spectra are in agreement with FIDASIM simulations on many fibers. Furthermore, the passive-FIDA spatial profile agrees with the simulation. When making measurements of active-FIDA in the edge region using time-slice subtraction, variations in the passive-FIDA contribution to the signal should be considered.

Keywords: passive FIDA emission, active FIDA emission, FIDASIM simulation

(Some figures may appear in colour only in the online journal)

## 1. Introduction

In magnetically confined fusion science, the study of fast-ion confinement and loss is essential because fast ions are usually a source of energy, momentum and particles in plasma. Furthermore, the fast-ion population and driven current influence macroscopic instabilities and plasma performance. Fast-ion loss can seriously damage the components of the first wall. Several diagnostics can supply information on the fast-ion population [1]. One appealing way is fast-ion D-alpha (FIDA) spectroscopy, which measures the Doppler-shifted Balmer-alpha line from the charge exchange (CX) reaction between the fast ions and neutrals [2–4]. In addition to the injected neutrals that are commonly used in FIDA measurements, background neutrals can also produce FIDA signal [5]. In this study, active-FIDA emission means the signal produced by CX between fast ions and injected beam neutrals, while passive fast-ion D-alpha (passive-FIDA) denotes radiation emitted by CX between fast ions and background neutrals.

In several tokamak devices, such as TCV [6], DIII-D [5, 7, 8], NSTX [5] MAST [9], and ASDEX Upgrade [10],

passive-FIDA measurements are discussed. These papers demonstrate that passive-FIDA is detectable, and is enhanced when fast ions are expelled to the edge by instabilities. Passive-FIDA measurement may be a technique to monitor fast-ion dynamics in the edge without active beam injection. It can also provide information on the neutral density profile [8]. The present work extends these prior studies to the National Spherical Torus Experiment Upgrade (NSTX-U) spherical tokamak. The new results show that, in a spherical tokamak, passive-FIDA signals can be comparable to active-FIDA signals and that active-FIDA measurements that employ time-slice subtraction can be corrupted by passive-FIDA signals.

The rest of the paper is organized as follows. Section 2 shows the diagnostic and the experimental setup. Section 3 describes modeling of the passive-FIDA and active-FIDA signals. The observed signals have the expected time evolution, spectral shape, radial profile, and dependence on beam-injection geometry (section 4). Section 5 shows that, owing to temporal variation of the passive-FIDA signal, under some circumstances background subtraction using a reference view is preferable to time-slice subtraction. Conclusions are presented in section 6.

The [appendix](#) describes the method used to correct the data for scattered  $D_\alpha$  light.

## 2. FIDA diagnostic and experimental conditions

The NSTX-U is a spherical tokamak with small aspect ratio (major and minor radii are 95 and 65 cm, respectively). The equipped neutral beam power is up to 12 MW. The nominal magnetic field and the current are  $B_T \leq 1$  T and  $I_p \leq 2$  MA, respectively. In this study, the typical discharge (e.g. 205 080) is a deuterium plasma in a low-confinement mode in a limiter configuration. The magnetic field is  $B_T \simeq 0.63$  T and the flat-top current is  $I_p \simeq 0.65$  MA. In the flat-top phase, the central electron density and temperature are  $n_e = 1.2\text{--}1.4 \times 10^{19} \text{ m}^{-3}$  and  $T_e = 0.6\text{--}0.9$  keV, respectively. Detailed plasma parameters are shown in figure 1.

On NSTX-U, two groups of spectroscopic FIDA diagnostics are installed: vertical [11] and tangential views [12] labeled by v- and t-FIDA, respectively. The t-FIDA diagnostic is most sensitive to passing ions, while the v-FIDA is more sensitive to trapped ions. V-FIDA has operated since 2008, while t-FIDA began to acquire data during the NSTX-U 2016 experimental campaign. The spatial resolution of FIDA is about 5 cm [4]. The temporal resolution for v-FIDA is 10 ms, but, to avoid blurring, the light is blocked by a chopper wheel for about 2 ms during camera readout for each time window. For t-FIDA, a CCD camera with faster readout speed is employed. For checking the t-FIDA signals, 10 ms integration time was used for several discharges in the campaign, but all data presented here were acquired at 5 ms temporal resolution. In addition, for t- and v-FIDA, the full width half maximum of the 650.024 nm oxygen line are about 0.6 and 0.4 nm, respectively.

The collection lenses of t- and v-FIDA are mounted above the midplane and on the top of the tokamak (figure 2(a)), respectively. In order to monitor background emission, the t- and v-FIDA reference views are toroidally displaced to avoid intersecting the active beams (figure 2(b)). In this paper, the different viewing chords are labeled by their major radius at the midplane. It should be noted, however, that every line of sight (LOS) intersects the last closed flux surface and can measure passive-FIDA light from the edge.

The collected light is carried to the spectrometer. In the spectrometer box, wavelengths outside the 645–667 nm passband are cut off by a bandpass filter, and the light is dispersed by a transmission grating. Next, the bright emission from the cold  $D_\alpha$  is strongly attenuated by a strip (neutral density filter with 1% transmission). Finally, the image is demagnified to the CCD chip. The acquired data are automatically stored in the MDSplus tree. A correction for scattered light is applied to the data prior to physics analysis ([appendix](#)).

For both systems, the intensity calibration is based on absolute calibration of a single v-FIDA fiber with an absolutely calibrated black-body source. A white-plate calibration technique then provides the relative channel-to-channel

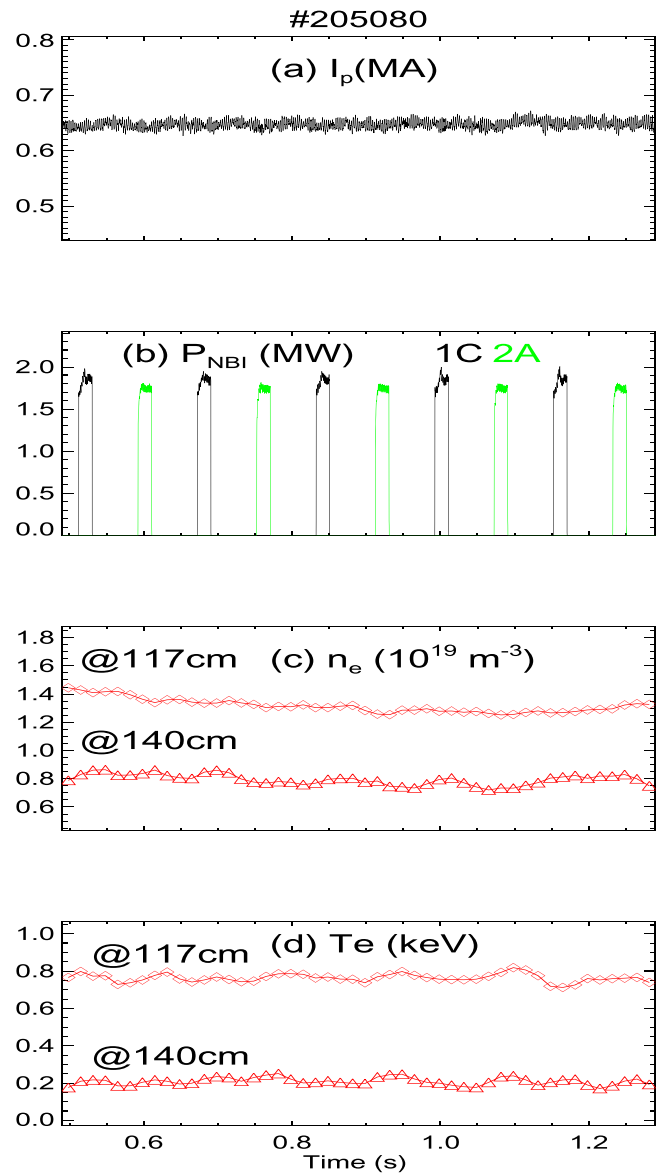


**Figure 1.** Time evolution of (a) plasma current, (b) injected beam power, (c) line-averaged electron density at inner (117 cm) and outer (140 cm) chords, and (d) electron temperature. Here, 117 and 140 cm correspond to flux surface  $\sqrt{\psi_p} = 0.43$  and  $0.87$ , respectively, with  $\psi_p$  being normalized poloidal flux.

calibration for all of the fibers in the v- and t-FIDA systems. The intensity of v-FIDA signal agrees with the FIDA simulation [13]. However, generally, the intensity of t-FIDA signal has a discrepancy with the FIDASIM simulation. In this study, we mainly concentrate on the comparison between the measured spectral shape and simulation. Hence, the FIDA-SIM simulation has been adjusted to match the intensity of the experiment results (section 3). Thus, the t-FIDA data are reliable for relative comparisons but not for absolute magnitudes.

On NSTX-U, one beamline uses three sources to inject 6 MW heating power inboard and the other beamline uses three sources to inject 6 MW outboard. The neutral beams are injected into the plasma from the midplane ports, and the

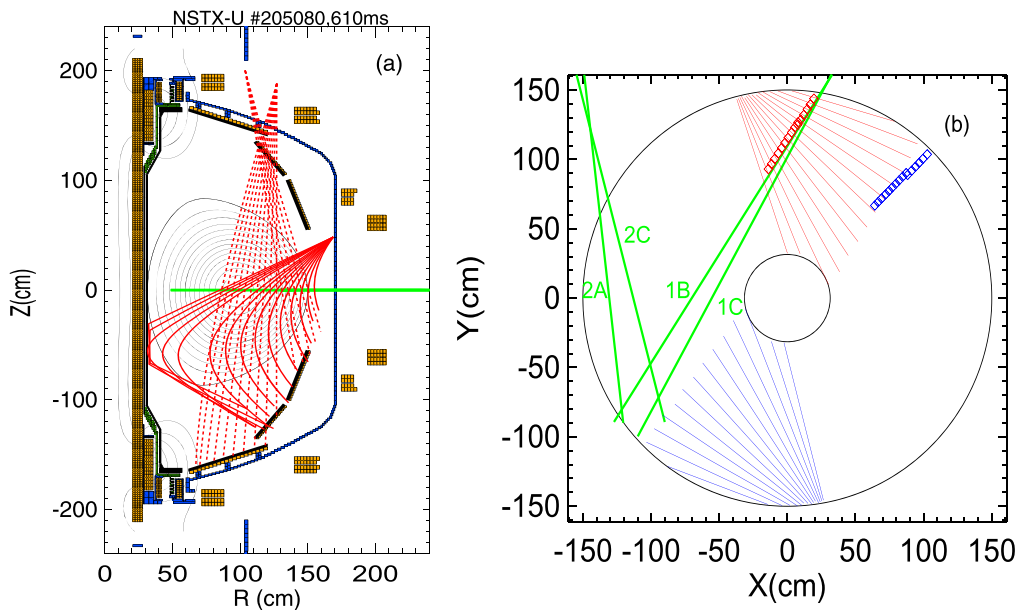


**Figure 2.** (a) Elevation and (b) plan view of the LOS of FIDA diagnostics. In (a), dashed and solid curves are the LOS of v/t-FIDA active view, respectively. In (b), symbols denote the v-FIDA LOS, while the solid curves label t-FIDA LOS. Red and blue denote the active view and reference view, respectively. T-FIDA active and reference views are tilted downward (a). The green lines show the centerline of inboard beam sources (1B and 1C) and outboard sources (2A and 2C), which are used as the diagnostic beam in this study.

injection is in the co-current direction. In this study, the outboard beam source 2A, 2C and inboard beam source 1B, 1C, with tangency radii of 130 cm, 110 cm and 60 cm, 50 cm are utilized (figure 2(b)). Inboard sources 1B and 1C produce signals in the active views. Based on the illustrated FIDA LOS, chords can be used to measure the passive-FIDA produced by either source. However, several reference views of t-FIDA in the edge region are contaminated by reflected light of beam emission. In addition, the passive-FIDA signals along the vertical view are weaker than the passive-FIDA signals in the tangential view. Hence, in this work, we concentrate on the t-FIDA active view (red solid curve in figure 2(b)).

Instabilities such as sawteeth and edge-localized modes can eject fast ions into the edge region [8, 9, 14–16], complicating the interpretation of the passive-FIDA signal. An L-mode quiescent discharge with short beam blips (20 ms beam-on for each blip) and high injected energy ( $\approx 85$  keV,  $P_{\text{NBI}} = 1.8$  MW) is employed in this study. MHD activity is weak in this discharge. The magnetic axis is about 99 cm for the studied shot. The time evolution of the plasma parameters is shown in figure 1. The current is approximately constant in the time window of interest. The electron density and temperature have a small variation during the discharge. In the chosen time window, 5-cycles of the beam modulation are employed. For most of the results shown in section 4, the signals are averaged over 5 cycles, as denoted in the figure caption.

### 3. FIDASIM modeling of active-FIDA and passive-FIDA signals

In general, the FIDA signal depends on the fast-ion distribution function, the neutral density profile, and the phase-space

sensitivity or ‘weight function’ of the particular FIDA view [17, 18, 19, 20]. Expected signals are predicted by the FIDASIM [21] synthetic diagnostic code. Since the discharges are MHD quiescent, the fast-ion distribution function is calculated by the TRANSP NUBEAM code [22] without any anomalous diffusion. Prediction of the active-FIDA signal is a standard application of FIDASIM: the NUBEAM distribution function is sampled and the light produced by CX between the fast ions and the injected and halo neutrals is computed.

Prediction of the passive-FIDA signal is less standard and more uncertain. One complication is the fast-ion distribution function. As shown in [8], in general, three distinct fast-ion populations can contribute to the passive-FIDA signal. One population is an axisymmetric population of fast ions that traverse the edge region. This population is accurately calculated by TRANSP and is employed here. The second population is a toroidally asymmetric cluster of fast ions that traverse the sightlines on their first orbits [5, 8]. Figure 3 shows a typical orbit born by the NSTX-U 2A neutral-beam source. Comparison with a similar graph from DIII-D (figure 3 of [5] or figure 1 of [23]) shows that the NSTX-U orbit is far less concentrated toroidally than a typical DIII-D orbit. Since this population is diffuse in NSTX-U and, in any event, its passive-FIDA spectrum closely resembles the spectrum produced by the axisymmetric population [8], this population is ignored here. The third population that can contribute to passive-FIDA light is centrally confined fast ions that are expelled to the edge region by instabilities. Since the present study is restricted to MHD-quiescent plasmas (except for the cases of modulating 1B and 2C, used in figure 6), this population is negligible.

The second complication is that, in contrast to the injected neutral population, the edge neutral population is

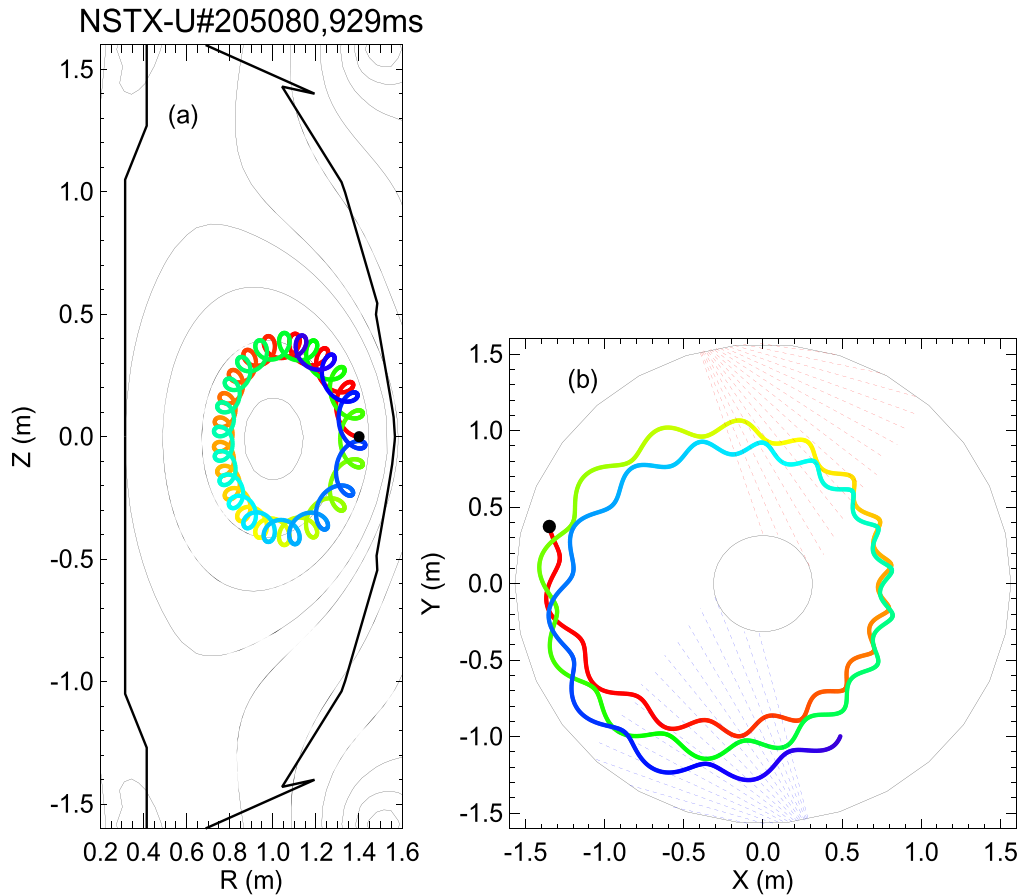


**Figure 3.** Orbit of an 83 keV fast ion born from the 2A source, with initial pitch  $v_{\parallel}/v = 0.9$  and initial position  $R = 140$  cm, which corresponds to the position in phase space of a local maximum with  $E = 83$  keV calculated by TRANSP.

poorly known. Accurate modeling of the edge neutral population is a challenge [24] due to the complicated nature of the wall components that act as neutral sources, to the sparse nature of neutral-density measurements, and to uncertainty in the temperature and density profiles in the scrape-off region. In its standard output, the TRANSP code includes a one-dimensional cold neutral-density profile [6]. The TRANSP calculation properly treats radial attenuation of edge neutrals as they penetrate into the plasma but treats toroidal and poloidal variations unrealistically; also, the actual value of the edge neutral density is quite uncertain. We adjust the particle confinement time  $\tau_p$  and the value of edge neutral density at the plasma boundary  $n_{\text{bdry}}$  in the TRANSP computation to check the variation of the predicted edge neutral distribution. The edge neutral density profiles for different cases are plotted in figure 4(a), and compared to measurements of an edge neutral density diagnostic (ENDD) [24] that is located near the midplane. In fact, the ENDD data varies substantially in time, which is mainly caused by the variation ( $\sim 5$  cm) of the plasma boundary during beam blips. In figure 4(a), we choose a good time point (1.135 s, beam-off phase), at which the case labeled by 205080H07 has reasonable agreement with the ENDD measurement. The FIDASIM simulation results used in this work are based on the 205080H07 neutral density profile. In addition, the dependence of the simulated passive-FIDA signal on the edge neutral density profile will be

presented later in figure 7(c). The TRANSP neutral-density profile is inserted into FIDASIM to estimate the passive-FIDA signal. Clearly, uncertainty in the neutral-density profile is the dominant uncertainty in comparison between the observed passive-FIDA signal and theory.

Figure 4(b) shows the fast-ion density profile calculated by TRANSP for a typical case. The guiding-center density is quite low near the plasma edge where the neutral density is large; nevertheless, owing to the large gyroradius of fast ions in a spherical tokamak, fast-ion orbits do traverse the edge, so the predicted passive-FIDA signal is appreciable.

#### 4. Passive FIDA measurement

This section shows that the time evolution, spectral shape, and radial profile of the measured signals are consistent with the expected behavior of the passive-FIDA emission.

Figure 5 compares the integrated FIDA signal with the simulation. For both t- and v-FIDA, the experimental and modeled signals have excellent agreement for the chosen chord ( $R = 117$  cm). In the simulation of the active view signal, during inboard beam injection (IC source), the simulated signal includes the signal from both the injected beam neutrals and the background neutrals. At other time slices when IC is off, the simulated signal only includes the



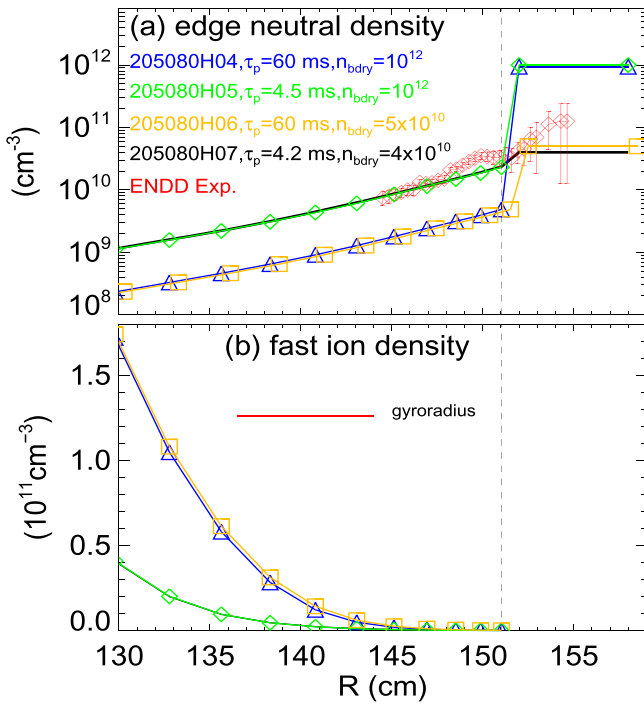


**Figure 4.** (a) Predicted edge neutral density at 1.135 s (beam-off phase) for the cases with different particle confinement time  $\tau_p$ . Edge neutral density amplitude  $n_{\text{bdry}}$  is set for 205080H07 and 205080H06, in order to roughly match the prediction and measured value from the edge neutral density diagnostic (ENDD) at the plasma boundary. The vertical dashed line denotes the plasma boundary. (b) Corresponding fast-ion density profiles and the gyroradius (red) of a typical fast ion.

contribution from the background neutrals. Since the modeled background neutral density and its spatial distribution have large uncertainty, the comparison of the amplitude of the experimental and simulated signal is not meaningful. However, the trend of the time evolution of the signals can be compared. In the comparison, the simulated passive signal is multiplied by a factor of 0.63 and 0.81 for t-FIDA and v-FIDA, respectively. This rescaling does not affect the trend of the time evolution of the simulated signal. It is clear from the figure that the passive-FIDA signal is comparable in magnitude to the active-FIDA signal.

Figure 5 also shows that the passive-FIDA light has the expected dependence on beam injection geometry. For v-FIDA the passive light is largest when the more perpendicular source (1C) is injected while, for t-FIDA, the signal is equally large when the more tangential source (2A) injects.

Usually, the passive contribution to the signal is larger for the tangential views than for the vertical views.

The excellent agreement between theory and experiment shown in figure 5 is not observed on every channel. The majority of t-FIDA chords show good agreement with theory but some of the v-FIDA channels have relatively poor agreement. Inaccuracies in the poloidal variation of the modeled neutral density are a likely cause of these differences. (The v-FIDA chords span a different range of poloidal angles than the t-FIDA chords.)

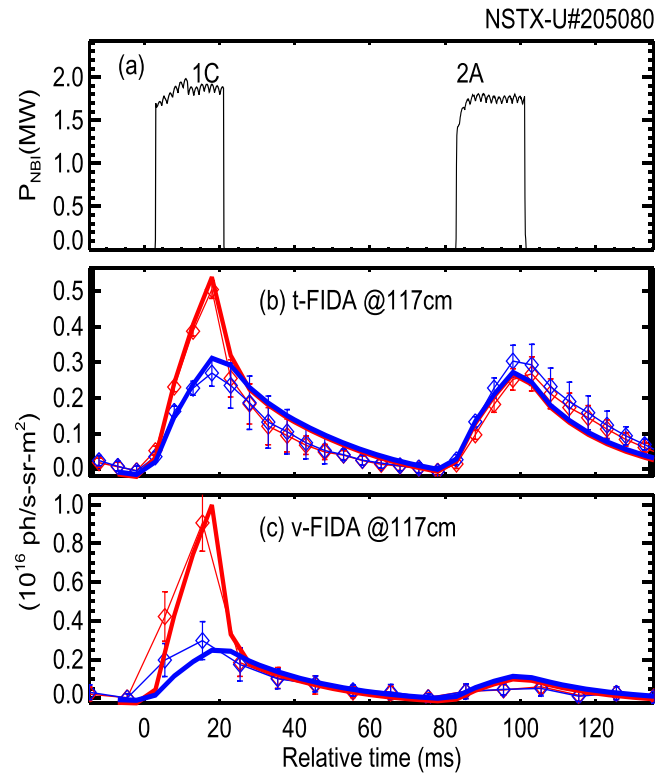


**Figure 5.** (a) Beam injection power, cycle-averaged FIDA signal for (b) t-FIDA and (c) v-FIDA at  $R = 117$  cm. The red and blue curves with error bars are the measured FIDA signal from active and reference view chords of each diagnostic system, respectively. The thick red and blue solid curves denote the FIDASIM predicted result using ‘injected plus edge’ and ‘only edge’ neutrals, respectively. The simulated result is rescaled to the experimental measurement. For simulated active t-FIDA and v-FIDA, the rescaling factors are 0.50 and 2.06, respectively, which are fixed in this work. For simulated passive t-/v-FIDA in (b) and (c), the rescaling factors are 0.63 and 0.81, respectively. The signal is integrated between 651 and 654 nm.

Database results (figure 6) show that the displayed behavior in figure 5 is representative. For t-FIDA, the passive-FIDA light is generally comparable to active-FIDA signal when the active beam sources (1B and 1C) are employed. Furthermore, the passive-FIDA signals for the more perpendicular sources (1B and 1C) are generally comparable to that for the more tangential sources (2A). While, for v-FIDA, the signals from 1C blips show the relatively weaker contribution of the passive-FIDA component to the total signal.

The measured passive-FIDA spectra agree with the FIDASIM prediction (figure 7). Source 2A does not produce any active light, only passive light. To isolate the passive-FIDA contribution from other possible contaminants to the spectrum, we subtract the averaged beam-off signal from the averaged beam-on signal for both the data and the theory. Here, the strong oxygen impurity line, at 650.024 nm, has been removed in the raw spectra prior to the subtraction. Two chords for beam blips of the 2A source are shown in figure 7. The measured spectra have the expected FIDA feature of approaching zero at wavelengths below 649.86 nm, which is the maximum possible Doppler shift for an 85 keV deuterium

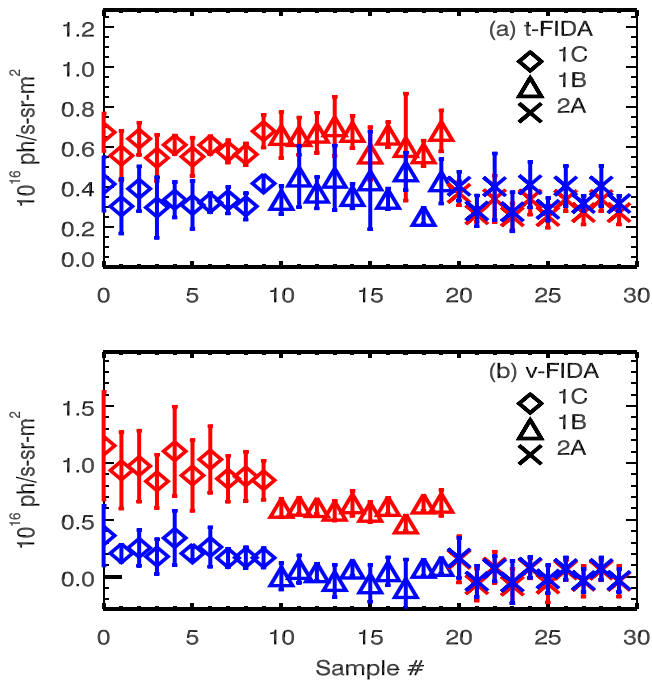


**Figure 6.** Database results from the blip shots. Each sample represents one time slice in the database. No cycle-average is carried out here. The symbols represent beam source 1C( $\diamond$ ), 1B( $\triangle$ ), and 2A( $\times$ ). (a) T-FIDA and (b) v-FIDA signals at  $R = 117$  cm. The red and blue symbols denote the measured signal at active and reference views, respectively. The signal is integrated between 651 and 654 nm.

ion. However, in some cases, the baseline (below 649.86 nm) still has a finite offset with respect to zero. This offset value is included as an additional error. The larger of the offset error and random error is plotted in the figures. Here, the random error normally denotes statistical error, while it denotes the combination of mean statistical error and standard deviation, when averaging over multiple cycles.

In addition, 7(c) shows that the shape of the passive-FIDA spectrum is insensitive to the variation of the edge neutral density profile. However, as expected, the amplitude of passive-FIDA increases (i.e. rescaling factor decreases) as the edge neutral density increases.

The spectra shown in figure 7 have an unusual shape that is consistent with the theoretical predictions. For a slowing-down distribution, the FIDA brightness increases monotonically with decreasing Doppler shift [13]. In the present case with a pulse train of beam blips, the fast-ion distribution has local maxima as shown in figures 8(a) and (c). The location of these maxima in velocity space depends upon the slowing-down time, beam modulation pattern, beam energy and beam orientation. Fast ions take longer to slow-down in the core than in the edge. As a result, the fast-ion distribution at  $R = 140$  cm (figure 8(a)) has a smaller tail towards lower energy than the one at  $R = 117$  cm (figure 8(c)). In addition, at  $R = 140$  cm, the fast ions with lower energy and smaller pitch values have relatively bigger contribution to FIDA emission than that at  $R = 117$  cm, as illustrated by the weight functions in figures 8(b) and (d). Hence, the bump features are less prominent on the  $R = 117$  cm channel than on the

$R = 140$  cm channel. The FIDASIM predictions successfully describe the measured bumps in the spectra.

The previous example is for outboard neutral-beam injection of the most tangential source. The measured spectral shape is also consistent with theory for inboard neutral-beam injection of the most perpendicular source. Figure 9 shows the measured spectra of the active and reference views of t-FIDA on two chords during inboard beam injection. At the edge chord ( $R = 140$  cm) (figures 9(a) and (b)), the experimental spectra agree with the FIDASIM prediction. In the simulation for the active view, both the injected and background neutrals are employed. In the simulation for the reference view, only the background neutrals' contribution is included. Interestingly, figure 9(c) shows that, at the 140 cm chord, the reference-view signal is almost equal to the active-view signal, which implies that the active-FIDA emission is almost zero. The signal is mainly from the CX interaction between the fast ions and the background neutrals. There also exists a slight decrease in the brightness for wavelengths  $> 653.2$  nm, which is due to the non-fully slowed-down distribution function of fast ions. By design, the active view is intended to measure the active-FIDA emission, and the reference view is intended to measure the background emission. Figure 9 clearly shows that, in practice, the passive-FIDA emission is large for both views.

At the inner chord ( $R = 117$  cm), figures 9(d) and (e) show that the simulated spectra agree with the measurement. Figure 9(f) demonstrates that in the 652–654 nm region (corresponding to fast ion energy components of 9.6–36.7 keV), the passive-FIDA signal is comparable to the active-FIDA signal. At the core region, the passive-FIDA contribution is about 50% of the total signal measured by the active view chord. Hence, for monitoring the passing fast-ion dynamics in time using the active beam method, the passive-FIDA contribution should be subtracted for inboard beam injection.

In addition, although the signals are considerably smaller, the red-shifted spectra are also consistent with theoretical predictions (figures 10(a) and (b)). The t-FIDA sightlines are oriented so that the co-passing ions injected by the neutral beams are heading towards the lens, producing a blue Doppler shift (figure 2(b)). As a result, the amplitude of the blue-shifted signal (figures 9(d)–(f)) is 3–4 times larger than the red-shifted signal (figures 10(a)–(c)). Nevertheless, within the uncertainties, the shape of red-shifted spectra basically agree with theory.

The passive-FIDA radial profiles for different integration regions are shown in figure 11. The experimental profiles are in good agreement with the simulation. As expected, the passive-FIDA signal is larger at the edge, and increases with increasing major radius in the region  $R > 127$  cm.

## 5. Discussion

The data in section 4 show that, in NSTX-U, the intensity of passive-FIDA light is often comparable to the intensity of active-FIDA light. This is in contrast to DIII-D [8] where, in the

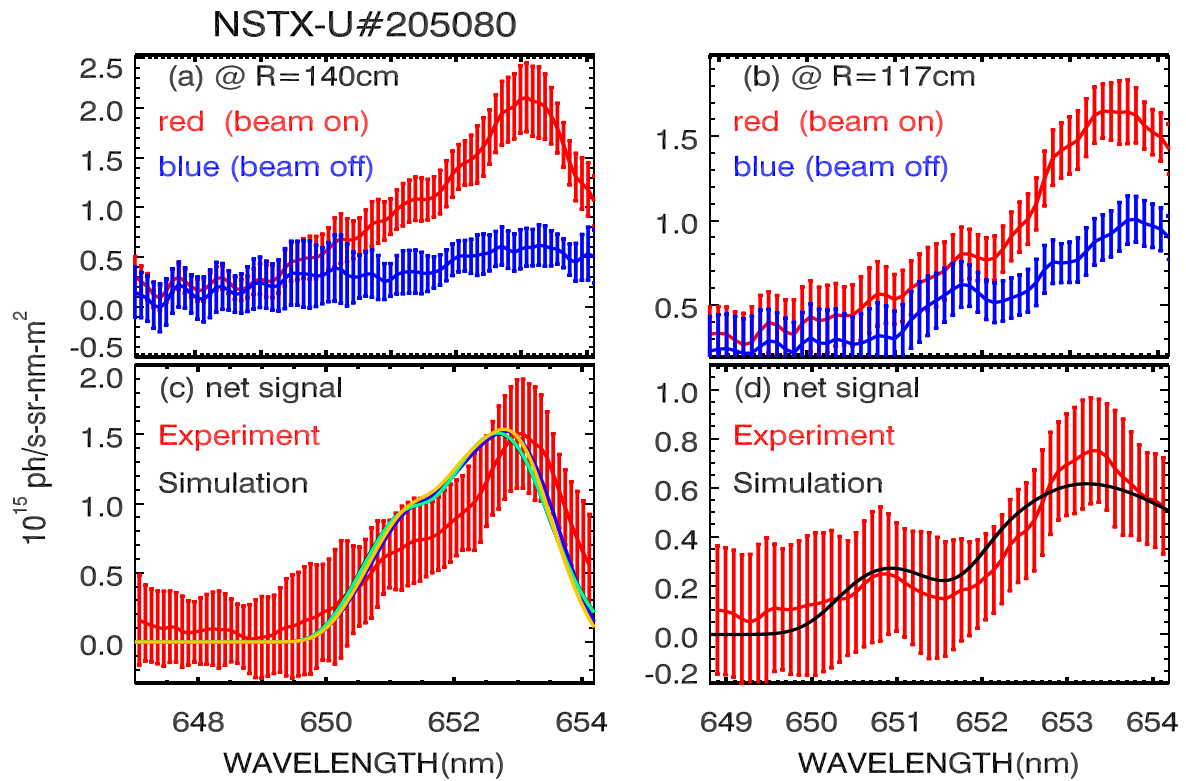


**Figure 7.** Cycle-averaged spectra of t-FIDA active view during beam-2A on (red) and 2A off (blue) at (a)  $R = 140$  cm and (b)  $R = 117$  cm. The experimental spectra are smoothed using a moving Gaussian instrument function with a width of 0.1 nm. The rescaling factor for four cases of 205080H04 (blue), 205080H05 (green), 205080H06 (yellow) and 205080H07 (black), are 1.08, 0.36, 1.27 and 0.35, respectively. Here, the black curve almost overlaps the green one. (c), (d) Difference between the beam-on and beam-off spectra (red), and the FIDASIM prediction (black). The average over multiple cycles is also carried out for the FIDASIM simulation. The simulation result is normalized to experiment, based on the assumption that the integrated signal in the shown wavelength region of FIDASIM equals the experimental value. The normalization factor is 0.33 in (d), in which the simulation is carried out based on the case 205080H07.

absence of instabilities that expel fast ions into the edge region, the passive signal is usually much smaller than the active signal. The likely reason for this difference is the relatively large gyroradius of fast ions in a spherical tokamak. Since the gyroradius is  $\sim 4$  times larger, a confined drift orbit is far more likely to traverse a region with large neutral density on a portion of its orbit than in DIII-D. In addition, in the conventional tokamak TCV, large passive FIDA signals have been observed in plasmas with large neutral densities [6].

The appreciable magnitude of the passive-FIDA emission has important implications for the optimal method of background subtraction. In DIII-D, timeslice subtraction is the preferred method of background subtraction; in ASDEX-Upgrade, the entire spectrum is modeled to extract the FIDA feature. These approaches are subject to appreciable errors when the passive FIDA emission is bright. If the spectrum is modeled, neglect of passive-FIDA light results in an overestimate of the active FIDA feature. If the passive-FIDA light is included in the modeling, uncertainties in the edge neutral density can cause appreciable errors.

When the modulation period is a significant fraction of the slowing-down time, timeslice subtraction is also prone to errors. Figure 12(a) compares two different methods of background subtraction for an edge chord. When the signal from the reference view is subtracted from the active view, the net signal is approximately zero. This differs from the

method of time-slice subtraction. If one subtracts the signal 10 ms after the beam turns off from the active-view signal when the beam is on, the net signal is positive. Naively, both of these methods should measure the active-FIDA signal and should therefore equal one another.

Figure 12(b) shows the reason for the discrepancy. In reality, the active-view signal contains a substantial contribution from passive-FIDA light. Since the distribution function changes on a 10 ms timescale in these discharges, the passive-FIDA signal is smaller 10 ms after the neutral-beam pulse than it is during the beam pulse. This difference is the source of the erroneous ‘active’ signal when using time-slice subtraction. In contrast, since the reference-view signal is acquired at the same time as the active-view signal, the passive-FIDA contribution is successfully removed when using reference-view subtraction. When using time-slice subtraction to determine the active-FIDA signal in the presence of time-evolving passive-FIDA contributions, care must be taken to correct for the temporal variation of the passive-FIDA signal.

In addition, although the shape of passive-FIDA spectrum is insensitive to the variation of edge neutral density profile as shown in figure 7, the amplitude of the simulated spectrum strongly depends on the amplitude of the edge neutral density. Furthermore, a larger edge neutral density (205080H05, 205080H07) induces a faster slowing down of fast ions (figure 13(b)), and produces relatively stronger passive-FIDA



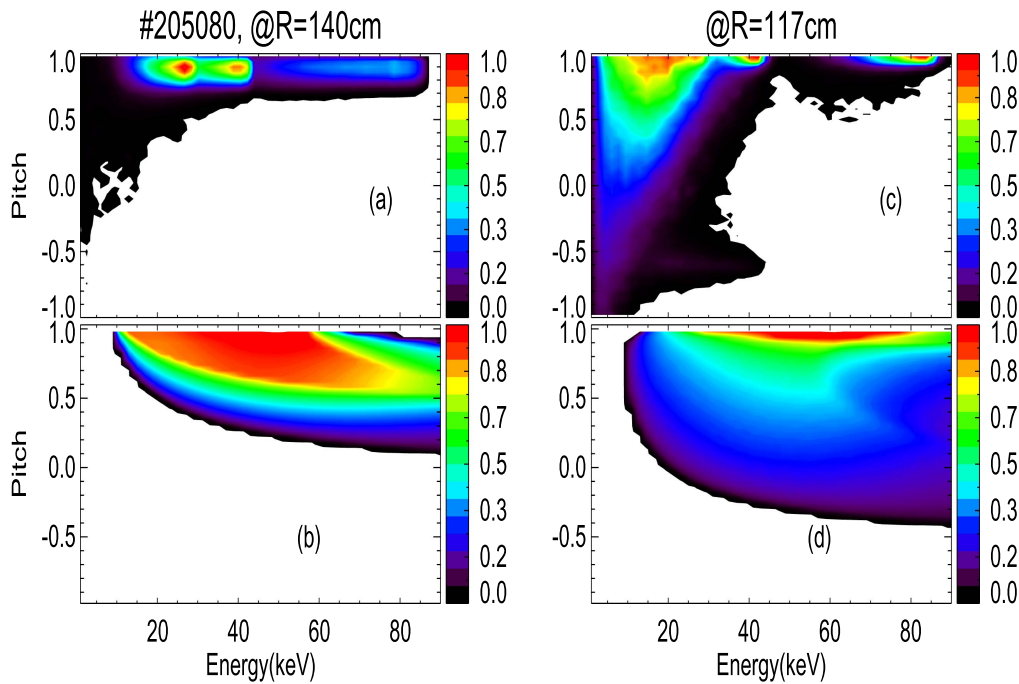


**Figure 8.** (a) Averaged (over five blips of the 2A source) classical fast-ion distribution function calculated by NUBEAM near the crossing of the t-FIDA sightline at  $R = 140$  cm with the midplane; (b) velocity-space sensitivity function of the t-FIDA active view at  $R = 140$  cm after integration between 651 and 654 nm; (c) and (d) show the fast-ion distribution function and the velocity-space sensitivity function for the inner chord at  $R = 117$  cm.

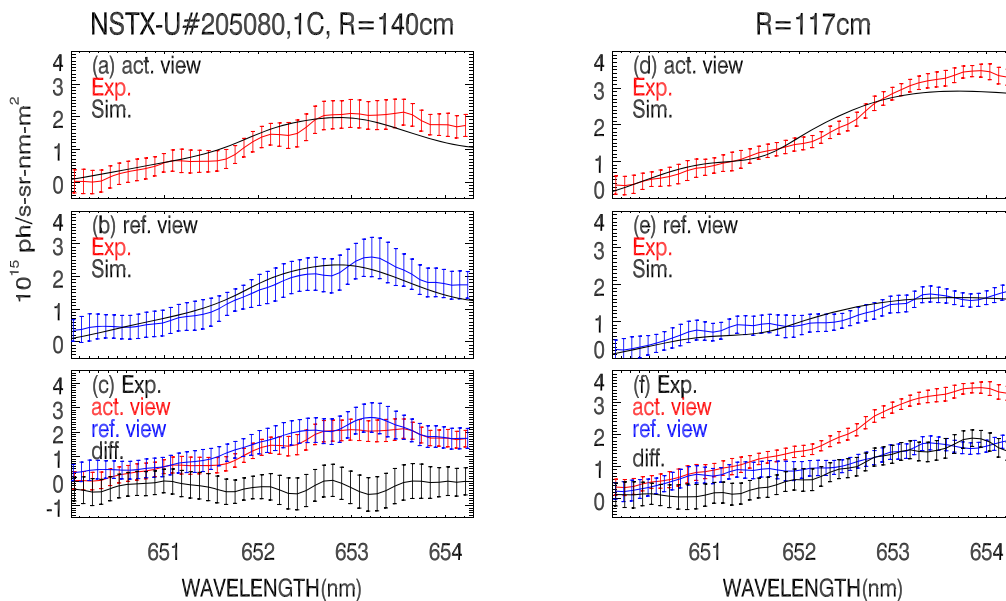


**Figure 9.** Comparison between the cycle-averaged FIDA spectra and the simulation for the inboard beam injection (1C source) case. In (a) and (b), the red and blue curves are the experimental spectra on active and reference chords (at  $R = 140$  cm) of t-FIDA, respectively. The black solid curve is the FIDASIM prediction. (c) Overlay of the active (red) and reference (blue) view signals together with their difference (black) which denotes the active FIDA signal. Panels (d)–(f) show the same quantities for the  $R = 117$  cm views. The FIDASIM predictions are rescaled, based on the assumption that the simulated total photons (integrated in the plotted spectral range) are equal to the experimental value. The rescaling factor for passive-FIDA are 0.38, 0.55, 0.58 and 0.56 in (a), (b), (d) and (e), respectively.

emission in the region 120–135 cm (figure 13(c)) than that in the cases with lower edge neutral density (dashed curves in figure 13(c)). Hence, it is suggested that the passive-FIDA measurement can be applied to infer the edge neutral density distribution, when the experimental data are of good quality.

## 6. Conclusion

Passive FIDA light makes a relatively large contribution to the total FIDA signal in NSTX-U. Four features of the signals are consistent with modeling of the passive-FIDA light.

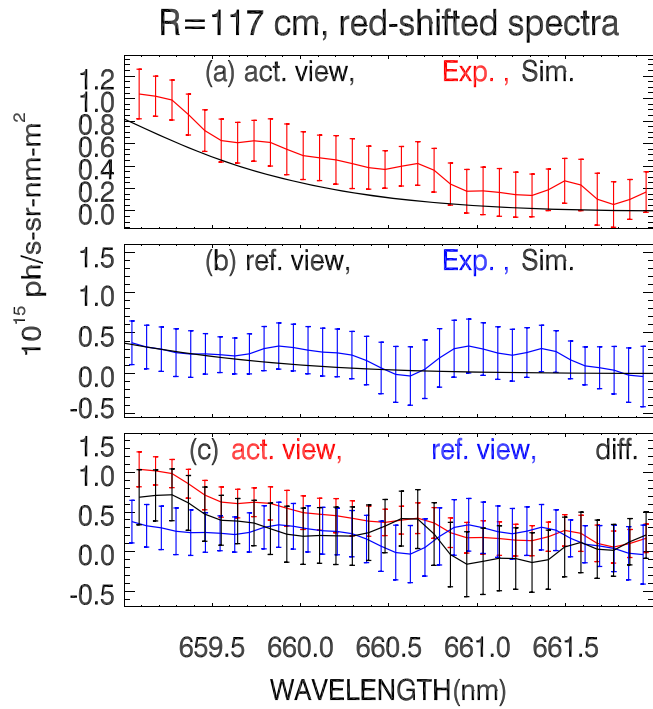


**Figure 10.** Red-shifted spectra at wavelengths above 656.1 nm at  $R = 117$  cm. In (a), the rescaling factors for simulated active and passive FIDA are 0.50 and 0.58 respectively. In (b), the rescaling factor for passive FIDA is 0.56.

- (i) The time evolution of the signals agree well with theory (figure 5).
- (i) The passive-FIDA signals show the expected dependence on beam injection angle (figure 5).
- (iii) The shapes of spectra agree with the theoretical prediction for both inboard (figure 9) and outboard (figure 7) injection.
- (iv) The radial profile agrees with theory (figure 11).

In summary, the passive FIDA signal is detectable for fast ions in the edge region. The passive FIDA technique may be employed to monitor the transport of fast ions in the edge region, as long as the bremsstrahlung emission at the edge is not too strong to drown out the FIDA emission. Improvements in the SNR of the measured signal through higher throughput optics (or other techniques) are desirable to obtain more precise information about the edge distribution function. In addition, when the passive-FIDA light is appreciable and time-evolving, a reference view is needed to measure the active FIDA emission. Otherwise, when time-slice background subtraction is used, modeling of the passive-FIDA signal should be employed together with accurate calculation of the edge neutrals. This will require a two- or three-dimensional calculation of the neutral density with, for example, the DEGAS code [24]. On the other hand, with good absolute calibrations for the experimental data, one could infer 2D neutral density profiles from the available data. This, however, is left for future work.

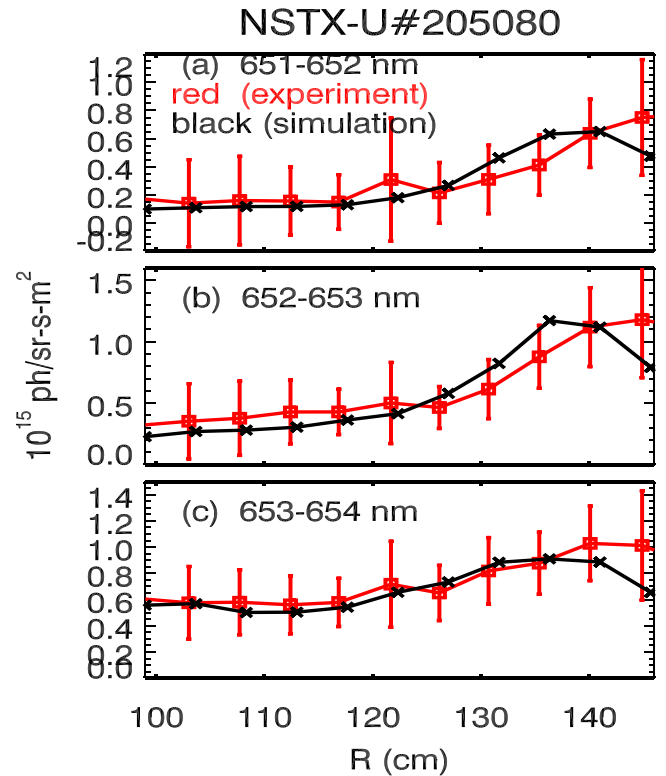


**Figure 11.** Comparison of the radial profile of the integrated FIDA signal between the experimental (cycle-averaged value) and FIDASIM prediction. Here, the signal is the difference between passive-FIDA when 2A is on and when it is off (20 ms after turning off 2A source). A five-cycle average is carried out. (a)–(c) show the results for the cases with different integration regions, as labeled in the figures. The FIDASIM predictions are rescaled, based on the assumption that the simulated total photons (integrated on radius for a given spectral range labeled in panel) are equal to the experimental value. The rescaling factors are (a): 0.25, (b): 0.28 and (c): 0.40.

## Acknowledgments

We thank the entire NSTX-U team for their support. This work is supported by the US DOE under Grant Nos. DE-AC02-09CH11466, DE-FG02-06ER54867, and DE-FG03-02ER54681. The digital data of this paper can be found at <http://dataspace.princeton.edu/jspui/handle/88435/dsp011v53k0334>.

## Appendix. Scattering correction

As discussed in detail in [13], on NSTX-U, contamination from scattered  $D_\alpha$  light is comparable to the FIDA signal, so a scattering correction is required to extract the FIDA emission. In this work, a scattering correction to the data from each individual view is carried out. We assume that the measured total signal  $T(i, \lambda, t)$  for the  $i$ th fiber in one exposure time interval  $t$  as a function of the wavelength  $\lambda$  can be written as:

$$T(i, \lambda, t) = P(i, \lambda, t) + S(i, \lambda, t) + A(i, \lambda, t). \quad (1)$$

Here,  $P(i, \lambda, t)$  is the background signal acquired by an individual fiber, which includes bremsstrahlung emission,

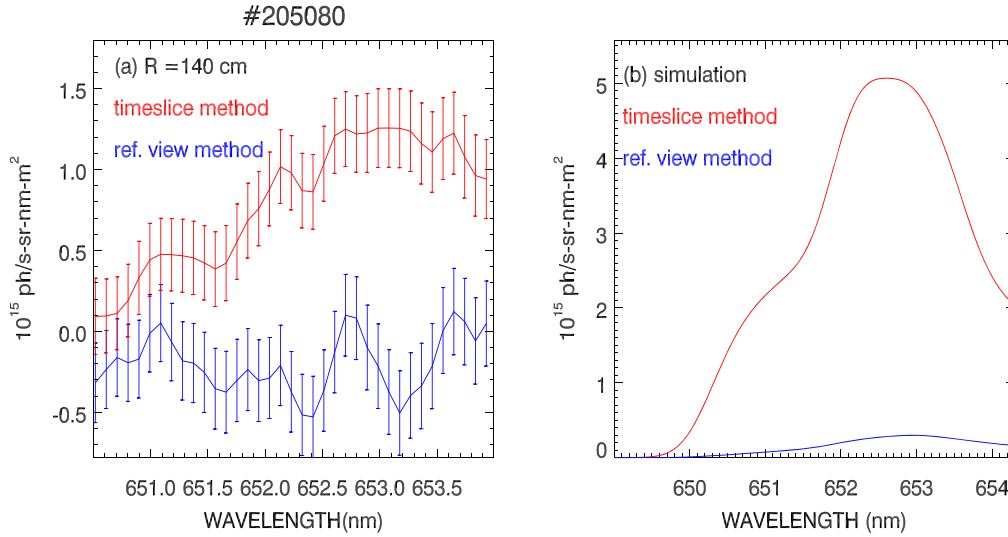


**Figure 12.** (a) Active FIDA signal for the  $R = 140$  cm t-FIDA chord using timeslice subtraction (red) and reference-view subtraction (blue) at 850 ms. The beam-off timeslice is from 860 ms. (b) Simulated active FIDA signal using the timeslice and reference-view subtraction methods. For the reference-view method, only the active-FIDA prediction is shown. For the timeslice method, the passive-FIDA prediction at 860 ms is subtracted from the sum of active-FIDA and passive-FIDA at 850 ms.

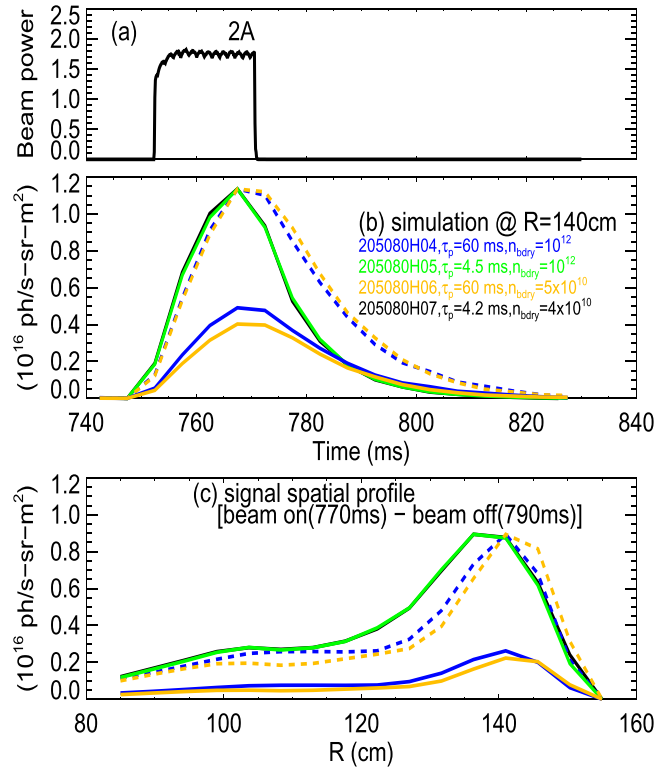


**Figure 13.** Time evolutions of simulated passive-FIDA signals (b) for a blip of 2A beam source (a), for different cases of the simulated edge neutral density profiles. (c) Corresponding spatial profiles of the simulated passive-FIDA signals during a beam blip. The results of cases (205080H04 and 205080H06) with lower edge neutral density are rescaled to the case of 205080H07, as plotted by dashed curves in (b) and (c). The signal is integrated between 651 and 654 nm.

passive-FIDA light, impurity line radiation, the cold  $D_{\alpha}$  line, and any other contamination.  $S(i, \lambda, t)$  is the scattered light, which depends on the wavelength.  $A(i, \lambda, t)$  is the active signal from active-FIDA, beam emission and halo emission

associated with active neutral beam injection. When the active beam is off,  $A(i, \lambda, t) = 0$ . The impurity lines are fitted and removed from the signal. To select a timeslice when passive-FIDA is negligible, we choose a (beam-off) time slice just before the next beam blip in each modulation cycle. The neutron rate in this time interval is  $<3\%$  of the peak value. Since the number of energetic ions is small, we assume that, in the wavelength region far away from the cold  $D_{\alpha}$  line, the measured signal consists entirely of scattered light and bremsstrahlung emission  $B(i, \lambda, t)$ . The measured signal at the  $i$ th fiber during the chosen beam-off time slice is

$$T(i, \lambda, t) = B(i, \lambda, t) + S(i, \lambda, t). \quad (2)$$

We assume that the contamination of scattered light to the individual view signal at each pixel is expressed by

$$S(i, \lambda, t) = \sum_{j=1}^{N_f} C(i, \lambda, j) \times I(j, t). \quad (3)$$

Here,  $C(i, \lambda, j)$  is the scattering correction coefficient and  $I(j, t)$  is the cold  $D_{\alpha}$  intensity on the  $j$ th fiber.  $N_f$  is the total number of fibers on the whole camera chip. Substituting equation (3) into (2) yields

$$0 = T(i, \lambda, t) - B(i, \lambda, t) - \sum_{j=1}^{N_f} C(i, \lambda, j) \times I(j, t). \quad (4)$$

The  $I(j, t)$  matrix is decomposed into a left matrix  $U$ , a diagonal matrix  $S$  and a right matrix  $V$ , as

$$I = USV^T, \quad (5)$$

where the superscript ' $T$ ' represents the transpose of the vectors. According to equations (4) and (5), the correction coefficient  $C$  is calculated by the matrix equation,

$$C(i, \lambda, j) = VS^+U^T[T(i, \lambda, t) - B(i, \lambda, t)]. \quad (6)$$


Here,  $S^\dagger$  is a diagonal matrix with the inverse of  $S$  in the diagonal. Once obtained, the correction coefficient  $C$  is applied to other time slices to extract the FIDA signal, using the formula,

$$A(i, \lambda, t) = T(i, \lambda, t) - B(i, \lambda, t) - \sum_{j=1}^{N_f} C(i, \lambda, j) \times I(j, t). \quad (7)$$

The bremsstrahlung emission is estimated by the FIDASIM simulation [13, 21]. This scattering correction is applied to both active and reference views of each FIDA system.

## ORCID iDs

G Z Hao  <https://orcid.org/0000-0003-2310-6134>

D Liu  <https://orcid.org/0000-0001-9174-7078>

M Podesta  <https://orcid.org/0000-0003-4975-0585>

A Bortolon  <https://orcid.org/0000-0002-0094-0209>

## References

- [1] Hutchinson I H 1987 *Principle of Plasma Diagnostics* (New York: Cambridge University Press)
- [2] Heidbrink W W, Burrell K H, Luo Y, Pablant N A and Ruskov E 2004 Hydrogenic fast-ion diagnostic using balmer-alpha light *Plasma Phys. Control. Fusion* **46** 1855
- [3] Luo Y, Heidbrink W W, Burrell K H, Kaplan D H and Gohil P 2007 Measurement of the D-alpha spectrum produced by fast ions in DIII-D *Rev. Sci. Instrum.* **78** 033505
- [4] Heidbrink W W 2010 Fast-ion D-alpha measurements of the fast-ion distribution (invited) *Rev. Sci. Instrum.* **81** 10D727
- [5] Heidbrink W W, McKee G R, Smith D R and Bortolon A 2011 Beam-emission spectroscopy diagnostics also measure edge fast-ion light *Plasma Phys. Control. Fusion* **53** 085007
- [6] Geiger B, Karpushov A N, Duval B P, Marini C, Sauter O, Andrebe Y, Testa D, Marascheck M, Salewski M, Schneider P A and The TCV Team The EUROfusion MST1 Team 2017 Fast-ion transport in low density l-mode plasmas at TCV using FIDA spectroscopy and the transp code *Plasma Phys. Control. Fusion* **59** 115002
- [7] Heidbrink W W *et al* 2011 Characterization of off-axis fishbones *Plasma Phys. Control. Fusion* **53** 085028
- [8] Bolte N G, Heidbrink W W, Pace D, Zeeland M V and Chen X 2016 Measurement and simulation of passive fast-ion D-alpha emission from the DIII-D tokamak *Nucl. Fusion* **56** 112023
- [9] Michael C A *et al* 2013 Dual view FIDA measurements on MAST *Plasma Phys. Control. Fusion* **55** 095007
- [10] Geiger B, Dux R, McDermott R M, Potzel S, Reich M, Ryter F, Weiland M, Wunderlich D and Garcia-Munoz M 2013 Multi-view fast-ion D-alpha spectroscopy diagnostic at ASDEX Upgrade *Rev. Sci. Instrum.* **84** 113502
- [11] Podesta M, Heidbrink W W, Bell R E and Feder R 2008 The NSTX fast-ion D-alpha diagnostic *Rev. Sci. Instrum.* **79** 10E521
- [12] Bortolon A, Heidbrink W W and Podesta M 2010 A tangentially viewing fast ion D-alpha diagnostic for NSTX *Rev. Sci. Instrum.* **81** 10D728
- [13] Hao G Z, Heidbrink W W, Liu D, Stagner L, Podesta M and Bortolon A 2017 On the scattering correction of fast-ion D-alpha signal on NSTX-U *Rev. Sci. Instrum.* submitted
- [14] Geiger B, Garcia-Munoz M, Heidbrink W W, McDermott R M, Tardini G, Dux R, Fischer R, Igochine V and The ASDEX Upgrade Team 2011 Fast-ion D-alpha measurements at ASDEX Upgrade *Plasma Phys. Control. Fusion* **53** 065010
- [15] Geiger B 2013 Fast-ion transport studies using FIDA spectroscopy at the ASDEX Update tokamak *PhD Thesis Ludwig-Maximilians-Universitat Munchen* 84, 113502
- [16] Jones O M, Michael C A, McClements K G, Conway N J, Crowley B, Akers R J, Lake R J, Pinches S D and The MAST Team 2013 Fast-ion deuterium alpha spectroscopic observations of the effects of fishbones in the mega-ampere spherical tokamak *Plasma Phys. Control. Fusion* **55** 085009
- [17] Heidbrink W W, Luo Y, Burrell K H, Harvey R W, Pinsker R I and Ruskov E 2007 Measurements of fast-ion acceleration at cyclotron harmonics using balmer-alpha spectroscopy *Plasma Phys. Control. Fusion* **49** 1457
- [18] Heidbrink W W, Bell R E, Luo Y and Solomon W 2006 Fast-ion D-alpha diagnostic for NSTX *Rev. Sci. Instrum.* **77** 10F120
- [19] Salewski M *et al* 2014 On velocity-space sensitivity of fast-ion D-alpha spectroscopy *Plasma Phys. Control. Fusion* **56** 105005
- [20] Stagner L and Heidbrink W W 2017 Action-angle formulation of generalized, orbit-based, fast-ion diagnostic weight functions *Phys. Plasmas* **24** 092505
- [21] Heidbrink W W, Liu D, Luo Y, Ruskov E and Geiger B 2011 A code that simulates fast-ion  $D\alpha$  and neutral particle measurements *Commun. Comput. Phys.* **10** 716–41
- [22] Pankin A, McCune D, Andre R, Bateman G and Kritz A 2004 The tokamak Monte Carlo fast ion module nubeam in the national transport code collaboration library *Comput. Phys. Commun.* **159** 157–84
- [23] Chen X, Austin M E, Fisher R K, Heidbrink W W, Kramer G J, Nazikian R, Pace D C, Petty C C and Van Zeeland M A 2013 Enhanced localized energetic-ion losses resulting from single-pass interactions with Alfvén eigenmodes *Phys. Rev. Lett.* **110** 065004
- [24] Stotler D P, Scotti F, Bell R E, Diallo A, LeBlanc B P, Podesta M, Roquemore A L and Ross P W 2015 Midplane neutral density profiles in the national spherical torus experiment *Phys. Plasma* **22** 082506